Journal of Applied Polymer Science

# Triglycine sulphate and its deuterated analog in polyurethane matrix for thermal/infrared detection: A comparison

**Jayalakshmy Maliyekattu Sudhakaran,[1] Jacob Philip[1,2]**

[1]Department of Instrumentation, Cochin University of Science and Technology, Cochin 682 022, Kerala, India

[2]Amal Jyothi College of Engineering, Kanjirappally, Kottayam 686 518, Kerala, India

Correspondence to: J. Philip (E-mail: jphilip6012@gmail.com)

**ABSTRACT:** Composites comprising of polycrystalline triglycine sulphate (TGS) or its deuterated analog (DTGS) in powder form dispersed in polyurethane (PU) are synthesized for pyroelectric sensor applications. TGS and DTGS have high pyroelectric coefficients, but are susceptible to humidity, and PU is inherently electroactive. So composites made of TGS or DTGS dispersed in PU can be expected to have high pyroelectric coefficient as well as immunity to humidity. Composites with inclusion volume fraction between 0 and 0.25 are prepared, and their dielectric, pyroelectric, and thermal properties measured. In general, deuteration leads to decrease in dielectric constant and specific heat, but increase in thermal conductivity. The pyroelectric coefficient and figures of merit get enhanced significantly with deuteration as well as inclusion volume fraction. Comparison with similar composites shows that these samples have the highest values for figures of merit, indicating their potential use as thermal/infrared detectors that are immune to humidity. © 2015 Wiley Periodicals, Inc. J. Appl. Polym. Sci. **2015**, *132*, 42250.

**KEYWORDS:** composites; dielectric properties; polyurethanes; sensors and actuators; thermal properties

Received 13 November 2014; accepted 22 March 2015

**DOI: 10.1002/app.42250**

## INTRODUCTION

Triglycine sulphate (TGS) crystal, with chemical formula $(NH_2CH_2COOH)_3H_2SO_4$, is a promising material for pyroelectric thermal/infrared sensor applications due to its high pyroelectric coefficient and relatively low dielectric constant. Pyroelectric sensors based on TGS are uniformly sensitive to radiation in wavelength range from ultraviolet to far infrared and do not require cooling for operation.[1–5] Pyroelectric IR detectors based on TGS family of crystals provide high figures of merit, but handling difficulties associated with their water solubility, hygroscopic nature and fragility have limited their use to single element detectors and vidicons, where sensitivity is of prime importance.[6–8] Moreover, the temperature range of operation of these crystals is very limited as the Curie temperature is rather close to room temperature.

In order to improve the ferroelectric and pyroelectric properties and to overcome the drawbacks cited above, many modifications to TGS have been proposed and evaluated for pyroelectric thermal/IR detection applications. One of these is deuteration of TGS.[9–12] Deuteration of TGS by dissolution and recrystallization in $D_2O$ produces $(ND_2CH_2COOD)_3{\cdot}D_2SO_4$, which is commonly referred to as partially deuterated TGS (DTGS). In fully deuterated TGS (FDTGS) with chemical formula $(ND_2CD_2COOD)_3.D_2SO_4$, the H atoms in the $CH_2$ group will also be replaced by deuterium.[13] Use of DTGS crystals allows to extend temperature range of sensing by 5–12°C due to their higher Curie temperature, depending on the deuteration level.[14,15] This increase in transition temperature on deuteration occurs because the hydrogen bonding in these materials play a dominant role in the ferroelectric transition mechanism.[16] From literature survey it can be inferred that deuteration of TGS provides a marked improvement in pyroelectric figures of merit of the material. Problems of humidity absorption, fragility, etc. exists for DTGS as well. In order to overcome these problems we tried to disperse these crystals in powder form in an electroactive polymer matrix and investigate their pyroelectric and related properties.

By dispersing these crystal powders in polymer matrix, their direct contact with air can be avoided and thus the problem of humidity absorption could be solved. Moreover, polymers can be processed easily into mechanically flexible and robust components. It is very difficult to achieve high enough pyroelectric/piezoelectric coefficients for composites formed by combining an ordinary polymer with pyroelectric/piezoelectric crystals. But there are many polymers that possess varying degrees of electroactivity. PVDF (Polyvinylidine diflouride) and its co-polymers like P(VDF–TrFE) (polyvinylidine diflouride–triflouro ethylene), P(VDF–HFP) (polyvinylidine difluoride–hexafluoro propylene),

PU (polyurethane), etc. are a few examples for electroactive polymers. Generally they have low pyroelectric/piezoelectric properties compared to crystals or ceramic materials possessing these properties. At the same time crystals as well as ceramics are very brittle, which is not often desirable for sensor fabrication. Moreover, TGS and DTGS crystals, which possess high pyroelectric coefficients, suffer from humidity absorption. So a good possible solution for the above problems is to combine these crystals with electroactive polymers to form composites. An important attribute of polymers is the ability to modify their inherent physical properties with addition of suitable fillers while retaining their many desirable mechanical properties.

In the present work we used the thermoplastic elastomer, polyurethane (PU), an electroactive polymer (EAP), as the matrix for fabricating composites with polycrystalline powders of TGS or DTGS as inclusions. Polyurethanes are unique polymers with a wide range of interesting mechanical, physical, and chemical properties. They are one of the most versatile classes of materials today and their demand as high performance industrial materials continue to grow. PU has a pyroelectric coefficient which is at least 2–4 times higher than that of PVDF, another popular electroactive polymer, and has a very low dielectric constant compared to PVDF.[17–20] PU is also famous for its toughness. This toughness comes from high flexibility and elongation of polyurethane chains. The PU polymer elastomer selected for this work is nonpiezoelectric and so does not generate piezoelectric noise by picking up vibrations from the environment. Moreover, the pliability of PU provides a cushion effect, which suppresses piezoelectric vibrations from TGS or DTGS crystallites in the composite. Vibration noise is undesirable for any piezoelectric material used for pyroelectric sensor applications. In this regard, the present polymer elastomer–ferroelectric crystal composite, having piezoelectric property, forms an alternative pyroelectric sensor material with higher signal to noise ratio. So by dispersing TGS and DTGS in PU matrix the drawbacks of these crystals in their pure form could be overcome and their composites in polymer possess advantages such as flexibility, toughness and immunity to humidity. These desirable properties qualify them for applications in hostile environments.

Pyroelectric thermal/infrared sensors are transducers for radiant energy. The detected energy in the form of temperature rise is transformed into electrical pulses proportional to the temperature difference between the surfaces of the detector. The uncooled pyroelectric infrared detectors are in great demand for many applications and a few of them are: atmospheric temperature measurement, earth position sensing, infrared detection, fire alarm operation, pollution detection, remote sensing, biomedical imaging etc.[17,21–25] One recent and important application is their use is in waste energy harvesting for microelectric generators.[26] In this paper, we discuss the properties of TGS/PU and DTGS/PU composites for pyroelectric infrared detection applications. A comparison of the pyroelectric properties of these two composites has been done and the experimental results are compared with theoretical predictions. Their properties are also compared with those of a few other ceramic–polymer composites possessing pyroelectric properties.

## MATERIALS AND METHODS

Small crystals of TGS were grown by conventional slow evaporation from solution at room temperature. The starting materials used were Glycine ($NH_2CH_2COOH$, Sigma-Aldrich) and Sulphuric acid ($H_2SO_4$, Merck). For the preparation, glycine and sulphuric acid were taken in a molar ratio 3 : 1, dissolved in double distilled water. It was necessary to increase the purity to a reputable level by successive recrystallization process and maximum attention was paid to secure high purity for TGS during synthesis. The partially deuterated TGS (DTGS) crystals were synthesised by recrystallization of pure TGS crystals in 99.9% heavy water ($D_2O$, Aldrich) more than six times. The polymer used in the present study was commercially available polyurethane (PU) transparent beads (Product code: P 2059) supplied by Otto Chemie.

Composite samples of TGS/PU and DTGS/PU were prepared in the form of free standing films by solvent cast method.[27] In this method, first, the required amount of polymer granules was dissolved in a suitable solvent (*N*, *N*-dimethyl formamide or DMF supplied by S D Fine Chem), and then the inclusion was added to it. The mixture was then stirred well. The inclusion crystals were made in to a fine powder before adding to the polymer solution. At most care should be taken to avoid agglomeration of the inclusion particles. This liquid composite was then poured into an open container of uniform depth of 1 mm for the solvent to evaporate completely. Finally, polymer composite was peeled off from the container in the form of a film. For all composites, 15 (w/v)% PU matrix solutions were used. For both cases, we have prepared films of TGS/DTGS volume fractions 0.001, 0.01, 0.05, 0.09, 0.15, and 0.25, including a pure PU film for comparison. From SEM images it was noticed that at 0.25 volume fractions of TGS or DTGS the inclusions started getting agglomerated (Figure 1). In order to avoid this problem we limited volume fractions of TGS/DTGS to 0.25. All the free standing films prepared were having thicknesses ranging from 35 to 85 μm for both set of composites.

The mass densities of the samples were measured by direct weighing method. The same were calculated theoretically from the densities of TGS/DTGS and PU following the rule of mixtures using the expression

$$\rho_{\text{eff}} = \varphi_f \rho_f + (1-\varphi_f)\rho_m \quad (1)$$

where $\rho$ and $\varphi$ are the density and volume fraction, respectively and the subscripts *m*, *f*, and *eff* stand for matrix, filler, and composite, respectively.

The important thermal properties for pyroelectric detectors, thermal conductivity, and specific heat capacity, were measured following a photopyroelectric (PPE) technique with a pyroelectric sensor used as the thermal detector.[28] Here the sample was in good thermal contact with the PVDF detector (coated with nickel–chromium alloy) of thickness 28 μm having pyroelectric coefficient 30 $\mu Cm^{-2}\ K^{-1}$. The sample detector assembly was mounted on a thermally thick copper backing. A 120 mW He–Cd laser of wavelength 442 nm, intensity modulated by a mechanical chopper, was used as the optical heating source. The modulation frequency of light was kept above 60 Hz to ensure

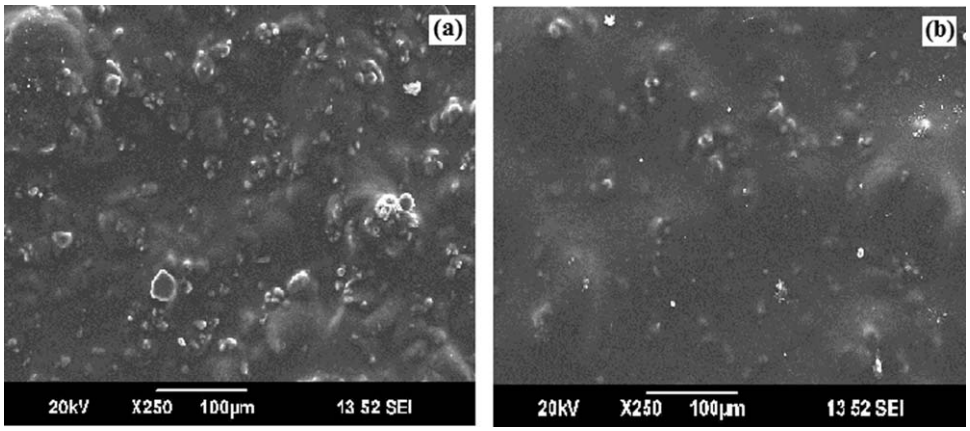


**Figure 1.** SEM images for (a) TGS/PU and (b) DTGS/PU composites, with inclusion volume fraction 0.25

that the detector, the sample and the backing were thermally thick during measurements. The output signal was measured with a dual-phase lock-in amplifier (Stanford Research Systems, Model: SR830). Measurement of amplitude and phase of the output signal enabled us to determine the thermal diffusivity ($\alpha$) and thermal effusivity ($e$), from which the thermal conductivity ($k$), and volume specific heat capacity ($C$) of the sample were obtained.

The theoretical values of thermal conductivity, specific heat capacity, and dielectric constant were calculated using the effective medium theory. The corresponding expressions used for the calculations are given below.[29–31]

$$\varphi_m \frac{k_m - k_{\text{eff}}}{k_m + 2k_{\text{eff}}} + \varphi_f \frac{k_f - k_{\text{eff}}}{k_f + 2k_{\text{eff}}} = 0 \quad (2)$$

$$C_{\text{eff}} = \varphi_f C_f + (1-\varphi_f) C_m \quad (3)$$

$$\varepsilon_{\text{eff}} = \varepsilon_m \frac{2\varepsilon_m + \varepsilon_f + 2\varphi_f(\varepsilon_f - \varepsilon_m)}{2\varepsilon_m + \varepsilon_f - \varphi_f(\varepsilon_f - \varepsilon_m)} \quad (4)$$

Here $\varepsilon$ is the dielectric constant. Since the assumptions of the effective medium theory are well documented in the cited references, they are not discussed any further here.

For dielectric and pyroelectric measurements, small pieces of dry films having area 1 $cm^2$ were coated with silver paste on both sides. The dielectric constant and dielectric loss of the samples were measured directly using an Impedance analyzer (Hioki, Model: IM3570) in the frequency range 100–5 MHz. The measured variations of dielectric constants were compared with the corresponding theoretical variations, determined using eq. (4).

In order to enhance the pyroelectric coefficients, both sets of samples were poled using corona poling technique. Samples in circular shape having diameter 4 cm were uniformly poled by a single corona point under a high DC electric field of 8 MV $m^{-1}$ at 75°C. Here all the samples were kept at the same temperature under the electric field for 40 min and then the temperature source was switched off maintaining the field while cooling the samples to room temperature.

The working principle of thermal/pyroelectric IR detectors is that the absorbed heat energy results in a corresponding increase in temperature ($dT$) and spontaneous polarization of the material. Changes in polarization alter the surface charge of the electrodes and to keep neutrality charges are expelled from the surface which results in a pyroelectric current ($I$) in an external circuit. The pyroelectric current is directly proportional to the temperature change with time ($dT/dt$) and the electrode area $A$ of the sample. The pyroelectric coefficients of the prepared samples were determined by the Byer and Roundy method, by keeping the heating/cooling rate at 2°C $min^{-1}$.[32] In order to calculate the pyroelectric coefficient $p(T)$ we used the expression:

$$p(T) = \frac{I}{A} \times \frac{1}{dT/dt} \quad (5)$$

PU used in the study fall under the category of thermoplastic polymers. Filler materials in the form of powders or fibbers can be added to thermoplastics to provide improvement of their specific properties like strength, stiffness, lubricity, etc. Hardness of polymers (rubbers/plastics) is usually measured by the Shore scales. Shore hardness is an empirical measurement used to test a polymer's resistance to indentation or penetration under a defined force. Two letters are used to categorize the type of PU: 'A' denotes a flexible type of PU while '$D$' refers to more rigid

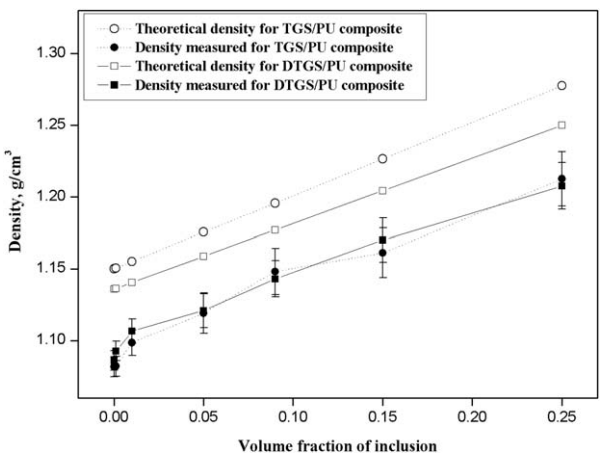


**Figure 2.** Variations of theoretical and experimental densities of TGS/PU and DTGS/PU composites with varying volume fractions of inclusions

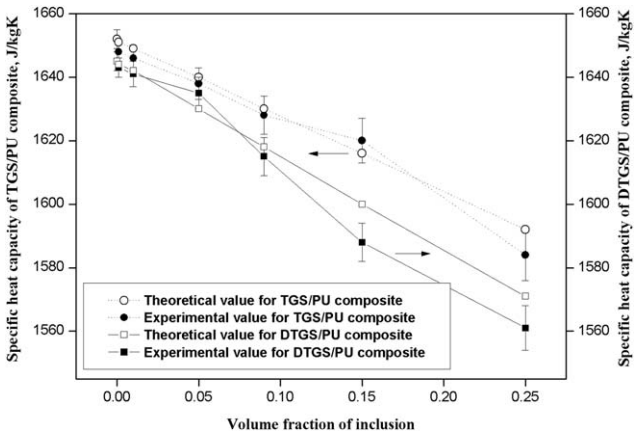


**Figure 3.** Variations of theoretical and experimental specific heat capacities of TGS/PU and DTGS/PU composites with volume fractions of inclusions

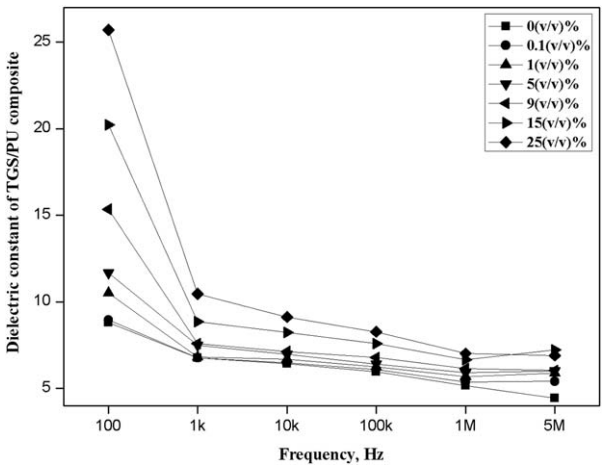


**Figure 5.** Variations of dielectric constant with frequency for different TGS/PU composites.

variety, i.e., the Shore A scale is used for 'softer' rubbers/plastics while Shore *D* scale is for 'harder' ones. These two categories can sometimes overlap. On both scales measurements range from zero to 100, with zero being very soft and 100 very hard. The Shore A hardness values for the samples, including pure PU, were measured following indentation method, measuring the penetration depth of a Durometer indenter with a Shore hardness meter (Hardmatic Mitutoyo, Model: 321JAA283). All measurements reported in this work have been carried out at normal environment [room temperature (28°C; relative humidity 70%)].

## RESULTS AND DISCUSSION

The SEM images of TGS/PU and DTGS/PU films shown in Figure 1 provide direct evidence for the presence of TGS or DTGS microcrystals in the polymer matrix.

The theoretical and experimental densities of the composites with varying volume fractions of TGS and DTGS are shown in Figure 2. It can be noticed that the density increases with filler concentration, and the experimental density is slightly lower than the theoretical density as the volume fraction increases. This is because of the possible presence of voids and defects present in the prepared composite films at higher filler concentrations. However, as the filler volume fraction increased from 0 to 0.25, all the prepared samples attained densities in the range 94–88% for TGS/PU and 95–90% for DTGS/PU composites.

Parameters to be considered for a pyroelectric sensor are its specific heat capacity and thermal conductivity. A good pyroelectric sensor is required to possess low specific heat capacity and low thermal conductivity. It is found that for TGS/PU composites the specific heat capacity, obtained from photopyroelectric measurements, decreases from 1652 to 1584 J $kg^{-1}$ $K^{-1}$with increase in filler concentration, whereas the corresponding thermal conductivity increases from 0.22 to 0.66 $Wm^{-1}$ $K^{-1}$. For DTGS/PU composites the specific heat capacity decreases from 1645 to 1561 J $kg^{-1}$ $K^{-1}$ with increase in filler concentration, while thermal conductivity increases from 0.26 to 0.90 $Wm^{-1}$ $K^{-1}$. The variations of specific heat capacity and thermal conductivity with filler concentration for both these composites, including theoretical predictions, are shown in Figures 3 and 4. Both these parameters for both sets of composites are in good

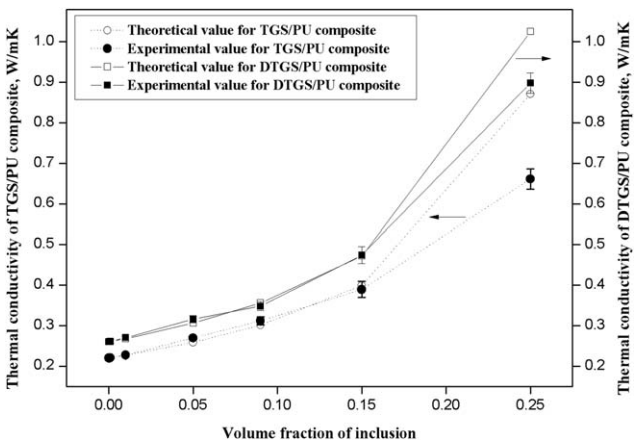


**Figure 4.** Variations of theoretical and experimental thermal conductivities of TGS/PU and DTGS/PU composites with volume fractions of inclusions

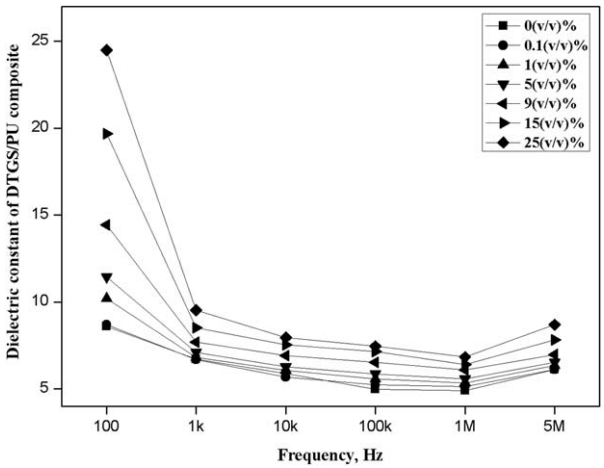


**Figure 6.** Variations of dielectric constant with frequency for different DTGS/PU composites.

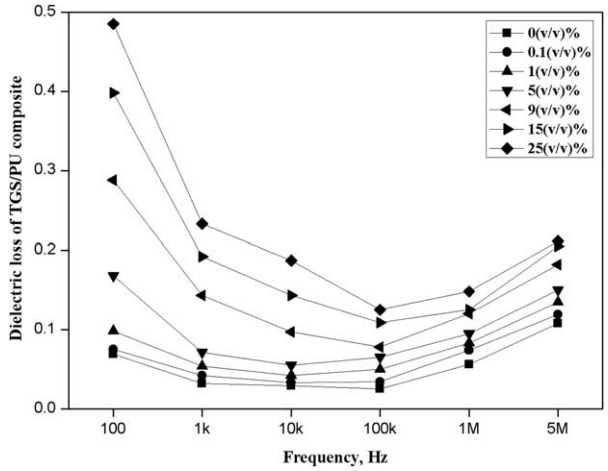


**Figure 7.** Variations of dielectric loss with frequency for different TGS/PU composites.

agreement with theoretical values, except at high filler concentrations. It is found that, in general, the deviations between theoretical and experimental values of thermal conductivity and heat capacity increase as the filler concentration increases. Moreover, deuteration gives rise to significant decrease in specific heat capacity and increase in thermal conductivity for these composites.

Variations of dielectric constant and dielectric loss with frequency for samples with different concentrations of TGS and DTGS in PU are shown in Figures 5–8. It can be seen that at all frequencies both dielectric constant and loss increase as TGS and DTGS contents in PU matrix increase. For TGS/PU the dielectric constant increases from 6.75 to 10.46 as the volume fraction of TGS increases from 0 to 0.25 at 1 kHz, and for DTGS/PU composites the corresponding variation is from 6.7 to 9.52. The increase in dielectric constant with increase in filler content can be attributed to enhancement in internal polarization of the samples. In the case of dielectric loss the corresponding variations for TGS/PU are from 0.03 to 0.23 and for DTGS/PU composites loss varies from 0.04 to 0.23. For both

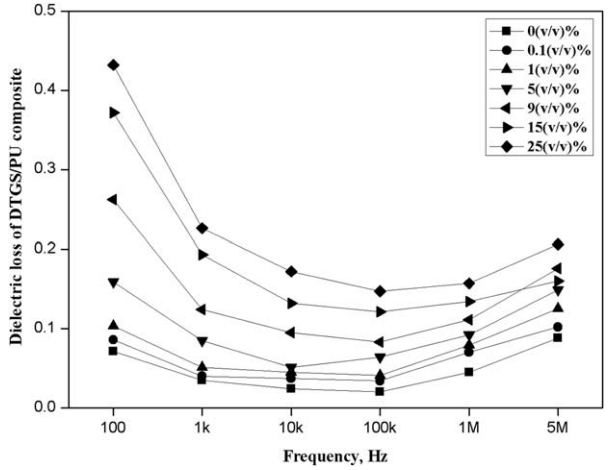


**Figure 8.** Variations of dielectric loss with frequency for different DTGS/PU composites.

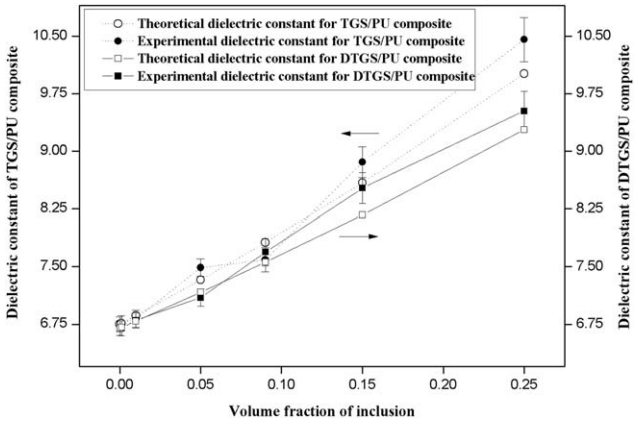


**Figure 9.** Variations of theoretical and experimental dielectric constants at 1 kHz for TGS/PU and DTGS/PU composites with volume fractions of inclusion.

the composites, dielectric constant and loss decrease as frequency increases. So from present measurements we can say that there is a slight decrease for dielectric constant for DTGS/PU composites compared to TGS/PU composites at higher filler concentrations, and that there exists no appreciable effect for

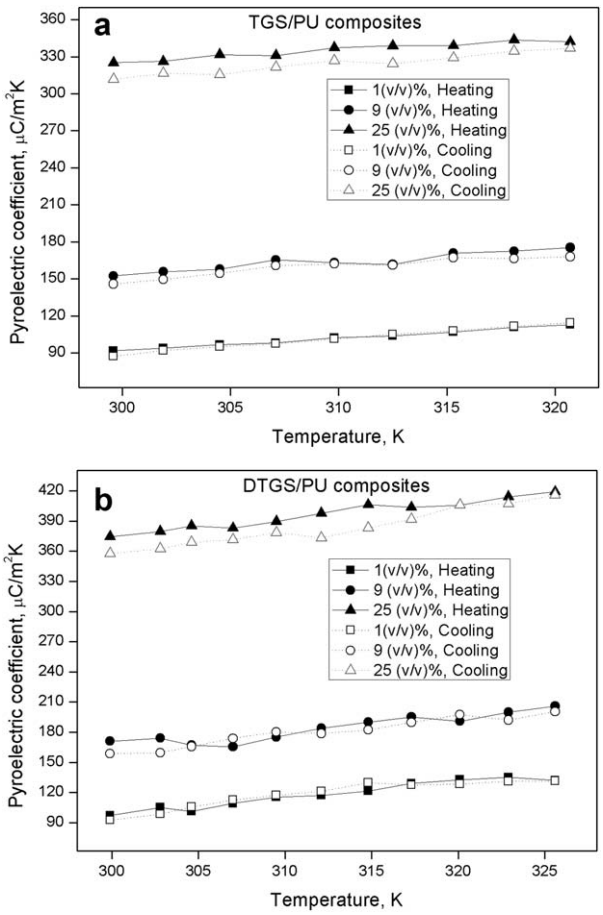


**Figure 10.** (a) Variation of pyroelectric coefficients of TGS/PU composites with temperature during heating and cooling; (b): variation of pyroelectric coefficients of DTGS/PU composites with temperature during heating and cooling.

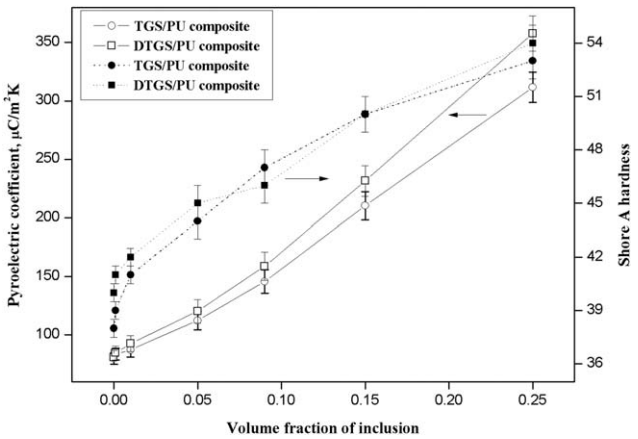


**Figure 11.** Variations of pyroelectric coefficients (cooling cycle) and Shore A hardness of TGS/PU and DTGS/PU composites with volume fractions of inclusion.

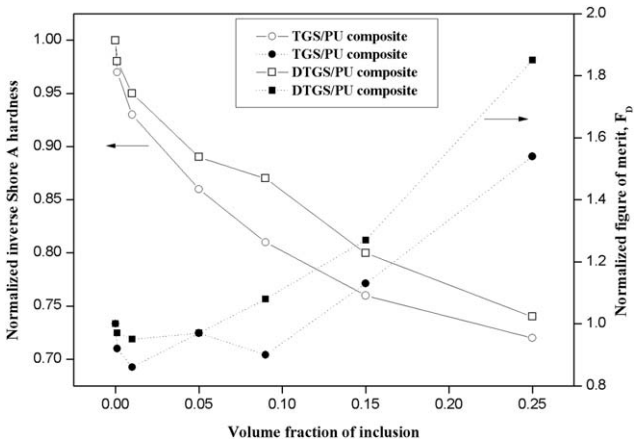


**Figure 12.** Variations of normalized pyroelectric figure of merit $F_D$ and normalized inverse Shore A hardness for TGS/PU and DTGS/PU composites with volume fraction of inclusion.

deuteration on the dielectric loss. A comparison with corresponding theoretical values for dielectric constants for TGS/PU and DTGS/PU composites are shown in Figure 9. From this figure, it is evident that the experimental results agree fairly well with theoretical values estimated from mean field theory.

Internal polarization of the composites increases due to contributions from inclusion dipoles. Enhancements in pyroelectric coefficients are obtained for the composite films after poling. Pyroelectric coefficients for all the samples were measured and verified during heating as well as cooling cycles (Figure 10). During heating, in addition to the pyroelectric current, a small current due to release of trapped space charges will be present. But during cooling the presence of depolarization currents can be eliminated. Figure 11 shows the variation of pyroelectric coefficients during cooling for varying volume fractions of TGS/DTGS in PU matrix. It is found that the average values of pyroelectric coefficients increase from 80 to 311 $\mu Cm^{-2} K^{-1}$ as the TGS concentration in the PU matrix increase from volume fraction 0 to 0.25 and the corresponding variation for DTGS/PU composites is from 80 to 357 $\mu Cm^{-2} K^{-1}$. At higher volume fractions of inclusions, the pyroelectric coefficient increases because of the presence of higher proportions of pyroelectric materials. But when compared to the pyroelectric coefficient for volume fraction 0.25 of TGS/PU composite, the value for DTGS/PU composite is only 357 $\mu Cm^{-2} K^{-1}$. This value is lower than expected. The reason may be that in the case of ferroelectric crystals that are pyroelectric, there is a possibility for a single domain crystal to become multidomain one during application, leading to reduction of internal polarization in the sample.[33]

The most important properties to look for in thermal/infrared sensor materials are their figures-of-merit. In order to improve the figures-of-merit the sensor materials should possess low dielectric constant and loss, high pyroelectric coefficient, low specific heat capacity and thermal conductivity. The important figures-of-merit for pyroelectric infrared detector materials are[34–37]

$$F_I = \frac{p(T)}{C},\ F_V = \frac{p(T)}{C\varepsilon},\ \text{and}\ F_D = \frac{p(T)}{C\sqrt{\varepsilon'}} \tag{6}$$

where $F_I$, $F_V$, $F_D$, are the figures-of-merit for high current sensitivity, high voltage responsivity, high detectivity, respectively, and $\varepsilon$' is the dielectric loss. The signal to noise performance of

**Table I.** Comparison of Figures of Merit for Thermal/IR Detection for TGS/PU and DTGS/PU Composites

| | TGS/PU composite | | | DTGS/PU composite | | |
|---|---|---|---|---|---|---|
| Volume fraction of inclusion | $F_I$ ($\times 10^{-3}$ $\mu Cm\ J^{-1}$) | $F_V$ ($\times 10^{-3}$ $\mu Cm\ J^{-1}$) | $F_D$ ($\times 10^{-3}$ $\mu Cm\ J^{-1}$) | $F_I$ ($\times 10^{-3}$ $\mu Cm\ J^{-1}$) | $F_V$ ($\times 10^{-3}$ $\mu Cm\ J^{-1}$) | $F_D$ ($\times 10^{-3}$ $\mu Cm\ J^{-1}$) |
| 0.00 | 48.42 ± 3.11 | 7.17 ± 0.56 | 270 ± 30 | 49.84 ± 3.74 | 7.43 ± 0.67 | 266 ± 32 |
| 0.001 | 50.97 ± 3.13 | 7.53 ± 0.57 | 248 ± 24 | 51.73 ± 3.75 | 7.73 ± 0.67 | 258 ± 29 |
| 0.01 | 54.07 ± 3.78 | 7.92 ± 0.68 | 232 ± 27 | 57.28 ± 4.41 | 8.42 ± 0.78 | 253 ± 30 |
| 0.05 | 70.20 ± 5.10 | 9.38 ± 0.83 | 263 ± 29 | 75.22 ± 6.35 | 10.60 ± 1.07 | 258 ± 30 |
| 0.09 | 91.52 ± 6.49 | 12.05 ± 1.11 | 242 ± 22 | 101.54 ± 7.82 | 13.20 ± 1.34 | 288 ± 29 |
| 0.15 | 133.33 ± 8.00 | 15.06 ± 1.25 | 304 ± 23 | 149.24 ± 8.76 | 17.51 ± 1.45 | 339 ± 25 |
| 0.25 | 200.75 ± 9.24 | 19.21 ± 1.42 | 415 ± 26 | 233.82 ± 10.68 | 24.56 ± 1.80 | 491 ± 29 |

**Table II.** Comparison of Figures of Merit for Thermal/IR Detection for TGS/PU and DTGS/PU Composites with Those Reported on Similar or Comparable Composites

| Material | Dielectric constant | Pyroelectric figures of merit | | | References |
|---|---|---|---|---|---|
| | | $F_I$ ($\mu Cm^{-2} K^{-1}$) | $F_V$ ($\mu Cm^{-2} K^{-1}$) | $F_D$ ($\mu Cm^{-2} K^{-1}$) | |
| PU (room temperature) | 6.7 | 49* | 7.43* | 266* | (present work) |
| TGS (room temperature) | 20–100 | 160–450 | 5–11.4 | 40–121 | 5 |
| DTGS (at 25°C) | 18–22.5 | 250–700 | 14 | – | 5 |
| $TGS_{(0.25\ vol.\ fraction)}$/PU (room temperature) | 10.45 | 318* | 30.41* | 658* | (present work) |
| $DTGS_{(0.25\ vol.\ fraction)}$/PU (room temperature) | 9.52 | 365* | 38.32* | 767* | (present work) |
| $DTGS_{(40\ wt\ \%)}$/PVDF (at 36°C) | 14.4 | 499 | 33.5 | 409 | 39 |
| $PT_{(0.54\ vol.\ fraction)}$/$P(VDF-TrFE)_{70/30}$ | 55 | 68.2 | 1.24 | 49.4 | 40 |
| $TGS_{(0.43\ vol.\ fraction)}$/P(VDF-TrFE) | 12.27 | 102 | 8.31 | 325 | 41 |
| $DTGS_{(5\ wt\ \%)}$/PVDF | 15.9 | 38.3 | 2.4 | 32.1 | 42 |
| PCLT/P(VDF-TrFE) | 15 | 56.5 | 3.7 | 113.2 | 43 |
| $PCaT_{(0.1\ vol.\ fraction)}$/P(VDF/TrFE) | 18 | 40 | 2.2 | 74 | 44 |
| $PCaT_{(0.50\ vol.\ fraction)}$/PEKK | 26 | 17 | 0.68 | 31.5 | 45 |
| $PZT_{(0.20\ vol.\ fraction)}$/P(VDF-TrFE) | 29 | 92 | 3.17 | 498.94 | 46 |

*Values are calculated using the same equations for figures of merit, but without division by specific heat capacity values for direct comparison with other reported results.

a pyroelectric material is determined by its detectivity. So, the most relevant figure-of-merit that weighs the material properties for optimal signal to noise ratio is $F_D$. All these figures-of-merit have been calculated for both TGS/PU and DTGS/PU composites and found that the figures-of-merit increase with increase of filler concentration. The values of these figures of merit for all the composites are tabulated in Table I. Variations of the figure of merit $F_D$, normalized to the corresponding one for pure PU, plotted against the volume fractions of TGS and DTGS crystal powders, are shown in Figure 12. It can be seen that the figure of merit increases more or less linearly with filler concentration, which is in tune with mean field approximation.[38] The other figures of merit also show similar kind of variations.

As shown in Figure 11, for TGS/PU as well as DTGS/PU composite films, Shore A hardness values increase with increasing volume fractions of inclusions. The variation of inverse Shore A hardness with varying volume fractions of TGS and DTGS are also shown in Figure 12 for a direct comparison with hardness. Since Shore hardness scales inversely with flexibility of the polymer, it is clear that the samples get harder (or flexibility decreases) as the inclusion concentration increases.

For TGS/PU composites, the inverse Shore hardness curves meet the figure of merit curves for high current sensitivity ($F_I$), high voltage responsivity ($F_V$), and high detectivity ($F_D$) at volume fractions 0.11, 0.11, and 0.14, respectively. At these points the TGS/PU composite possesses good flexibility as well as high figures of merit. For DTGS/PU the respective volume fractions are 0.13, 0.12, and 0.14. Only the plots of normalised $F_D$ versus inverse Shore A hardness curves for both TGS/PU and DTGS/PU have been included in the manuscript. These data provide guidelines for the selection of a suitable composite of this class for sensor applications.

In order to compare the pyroelectric properties of present TGS/PU and DTGS/PU composites with those of comparable composites reported in literature, we tabulate the relevant properties of a few composites in Table II. It can be seen that the present composites with TGS or DTGS volume fraction 0.25 have higher figures of merit than other similar or comparable composites reported in literature. So these can be considered as good choice for the design and fabrication of thermal and infrared sensors where the application demands materials that are immune to humidity.

## CONCLUSIONS

Efforts have been made to prepare composites of TGS and its deuterated analog in polyurethane matrix and investigate their pyroelectric properties so as to evaluate their use as thermal/infrared detectors. Experimental results on dielectric constant, thermal conductivity and specific heat capacity obtained for various inclusion volume fractions for both TGS/PU and DTGS/PU composites are compared with theoretical predictions and the values are found to be in good agreement. The pyroelectric figures of merit for IR detection for both sets of composites are compared with those of comparable composites reported in literature for the first time. It is found that TGS/PU and DTGS/PU composites with volume fraction 0.25 offer good choice of materials for the design and fabrication of thermal/IR sensors that can withstand humidity and other hostile environments.

## ACKNOWLEDGMENTS

The work was supported by DST, Government of India under Nanomission scheme (SR/NM/NS-30/2010). One of the authors (MSJ) thanks DST, New Delhi for a fellowship under

PURSE scheme. Sophisticated Analytical Instrument Facility (SAIF), STIC, Cochin is gratefully acknowledged for sample characterization.

## REFERENCES


1. Batra, A. K.; Currie, J. R.; Aggarwal, S. K.; Aggarwal, M. D.; Lal, R. B. Proc. SPIE **2003**, *5209*, 133.
2. Begum, S. N.; Sankar, U.; Thanu, T. C.; Selvarajan, P. *Optik* **2014**, *125*, 1493
3. Zhao, X.; Wu, X.; Liu, L.; Luo, H.; Neumann, N.; Yu, P. *Phys. Status Solid A* **2011**, *208*, 1061.
4. Nakatani, N. *Ferroelectrics* **2011**, *413*, 238.
5. Aggarwal, M. D.; Batra, A. K.; Guggilla, P.; Edwards, M. E.; Penn, B. G.; Currie, Jr. J. R. NASA/TM **2010**, 216373/1.
6. Jimenez, R.; Jimenez, B. *Springer Ser. Mater. Sci.* **2011**, *140*, 573.
7. Fang, C. S.; Wang, M.; Zhuo, H. S. *Ferroelectrics* **1989**, *91*, 373.
8. Capan, R. *BAÜ FBE Dergisi* **2010**, *12*, 75.
9. Sinha, N.; Goel, N.; Singh, B. K.; Gupta, M. K.; Kumar, B. *J. Solid State Chem.* **2012**, *190*, 180.
10. Raj, C. J.; Kundu, S.; Varma, K. B. R. *Appl. Phys. A* **2011**, *105*, 1025.
11. Rai, C.; Sreenivas, K.; Dharmaprakash, S. M. *J. Cryst. Growth* **2010**, *312*, 273.
12. Hudspeth, J. M.; Goossens, D. J. *J. Cryst. Growth* **2012**, *338*, 177.
13. Hudspeth, J. M.; Goossens, D. J.; Gutmann, M. J.; Studer, A. *J. Cryst. Res. Technol.* **2013**, *48*, 169.
14. Arago, C.; Menendez, L. G.; Gonzalo, J. A. *Ferroelectrics* **2014**, *462*, 47.
15. Hudspeth, J. M.; Goossens, D. J.; Welberry, T. R.; Gutmann, M. J. *J. Mater. Sci.* **2013**, *48*, 6605.
16. Loiacono, G. M.; Kostecky, G. *Thermochem. Acta* **1981**, *45*, 133.
17. Jayalakshmy, M. S.; Philip, J. *Sens. Actuators A: Phys.* **2014**, *206*, 121.
18. Sakamoto, W. K.; Kagesawa, S.; Kanda, D. H.; Das-Gupta, D. K. *J. Mater. Sci.* **1998**, *33*, 3325.
19. Frubing, P.; Kruger, H.; Goering, H.; Gerhard-Multhaupt, R. *Polymer* **2002**, *43*, 2787.
20. Lam, K. S.; Wong, Y. W.; Tai, L. S.; Poon, Y. M.; Shin, F. G. *J. Appl. Phys.* **2004**, *96*, 3896.
21. Yun, J.; Lee, S. S. *Sensors* **2014**, *14*, 8057.
22. Steffanson, M.; Rangelow, I. W. *Opto-Electron. Rev.* **2014**, *22*, 1.
23. Xiong, J.; Li, F.; Zhao, N.; Jiang, N. *Sensors* **2014**, *14*, 7209.
24. Li, L.; Zhao, X.; Li, X.; Ren, B.; Xu, Q.; Liang, Z.; Di, W.; Yang, L.; Luo, H.; Shao, X.; Fang, J.; Neumann, N.; Jiao, J. *Adv. Mater.* **2014**, *26*, 2580.
25. Siebke, G.; Holik, P.; Schmitz, S.; Schmitz, H.; Lacher, M.; Steltenkamp, S. *Bioinspir. Biomim.* **2014**, *9*, 036012/1.
26. Potnuru, A.; Tadesse, Y. *Integr. Ferroelectr.* **2014**, *150*, 23.
27. Sanchez-Garcia, M. D.; Gimenez, E.; Lagaron, J. M. *Carbohydr. Polym.* **2008**, *71*, 235.
28. Menon, C. P.; Philip, J. *Meas. Sci. Technol.* **2000**, *11*, 1744.
29. Rizvi, I. H.; Jain, A.; Ghosh, S. K.; Mukherjee, P. S. *Heat Mass Transfer.* **2013**, *49*, 595.
30. Han, Z. Nanofluids with Enhanced Thermal Transport Properties; Ph.D. Thesis, University of Maryland, College Park, Maryland, **2008**.
31. Hossain, M. E.; Liu, S. Y.; O'Brien, S.; Li, J. *Acta Mech.* **2014**, *225*, 1197.
32. Byer, R. L.; Roundy, C. B. *Ferroelectrics* **1972**, *3*, 333.
33. Nautiyal, A.; Upadhyay, T. C. *Int. J. Chem. Sci. Appl.* **2013**, *4*, 29.
34. Sidney, B. L.; Das-Gupta, D. K. *Ferroelectr. Rev.* **2000**, *2*, 217.
35. Whatmore, R. W.; Watton, R. Pyroelectric Materials and Devices. In 'Infrared Detectors and Emitters: Materials and Devices; Capper, P.; Elliott, C. T., Eds.; Kluwer Academic Publishers Group: The Netherlands, **2001**, p 99.
36. Rogalski, A. *Prog. Quant. Electron.* **2003**, *27*, 59.
37. Guggilla, P.; Batra, A. K.; Currie, J. R.; Aggarwal, M. D.; Alim, M. A.; Lal, R. B. *Mater. Lett.* **2006**, *60*, 1937.
38. Barber, P.; Balasubramanian, S.; Anguchami, Y.; Gong, S.; Wibowo, A.; Gao, H.; Ploehn, H. J.; Loye, H. C. Z. *Materials* **2009**, *2*, 1697.
39. Batra, A. K.; Simmons, M.; Guggilla, P.; Aggarwal, M. D.; Lal, R. B. *Integr. Ferroelectr.* **2004**, *63*, 161.
40. Chan, H. L. W.; Chan, W. K.; Zhang, Y.; Choy, C. L. *IEEE Trans. Dielect. Electr. Insul.* **1998**, *5*, 505.
41. Sreenivas, K.; Rao, T. S.; Dhar, A.; Mansingh, A. *Bull. Mater. Sci.* **1984**, *6*, 105.
42. Changshui, F.; Qingwu, W.; Hongsheng, Z. J. *Korean Phys. Soc.* **1998**, *32*, S1843.
43. Zhang, Q. Q.; Ploss, B.; Chan, H. L. W.; Choi, C. L. *Sens. Actuators A: Phys.* **2000**, *86*, 216.
44. Zhang, Q. Q.; Chan, H. L. W.; Ploss, B.; Zhou, Q. F.; Choy, C. L. *J. Non-Cryst. Solids* **1999**, *254*, 118.
45. Pelaiz-Barranco, A.; Martinez, O. P.; Das-Gupta, D. K. *J. Appl. Phys.* **2002**, *92*, 1494.
46. Dietze, M.; Krause, J.; Solterbeck, C.-H.; Es-Souni, M. *J. Appl. Phys.* **2007**, *101*, 054113/1.